REPORT SERIES IN AEROSOL SCIENCE
N:o 136 (2012)

ESTIMATING PARTICLE NUMBER SIZE DISTRIBUTIONS FROM MULTI-INSTRUMENT OBSERVATIONS WITH KALMAN FILTERING

Toni Viskari

Finnish Meteorological Institute
Climate Change
P.O. Box 503
00101 Helsinki, Finland

Academic dissertation

To be presented, with the permission of the Faculty of Science of the University of Helsinki, for public criticism in auditorium D101, Gustaf Hällströmin katu 2, on November 9th, 2012, at 12 o'clock noon.

Helsinki 2012

Author's Address: Department of Physics
P.O. Box 64
FI-00014 University of Helsinki
e-mail

Supervisors: Professor Markku Kulmala, Ph.D.
Department of Physics
University of Helsinki

Professor Heikki Järvinen, Ph.D.
Finnish Meteorological Institute

Reviewers: Professor Markus Olin, Ph.D.
Technical Research Centre of Finland
Professor emeritus Pertti Hari, Ph.D.
Department of Forest sciences
University of Helsinki

Opponent: Doctor Wolfram Birmili, Ph.D.
Leibniz Institute for Tropospheric Research

ISBN 978-952-5822-64-9 (printed version)
ISSN 0784-3496
Helsinki 2012
Unigrafia Oy
ISBN 978-952-5822-65-6 (PDF version)
http://ethesis.helsinki.fi/
Helsinki 2012
Helsingin yliopiston verkkojulkaisut

Acknowledgements

The research for this thesis was performed at the Climate Change Unit, Research and Development Division of the Finnish Meteorological Institute. I am grateful for the Institute, especially for the head of the Research and Development division Prof. Yrjö Viisanen, for providing me the working facilities and resources used while working on this thesis. I also express my gratitude for the unit leaders Professor Ari Laaksonen and Research Professor Heikki Järvinen for making the project possible and finding the funding for it. I am of course also thankful for the Academy of Finland for judging the project worth funding.

This research was done under the supervision of Professors Markku Kulmala and Heikki Järvinen. Professor Kulmala ensured that I could focus on my research and provided advice when it was needed. Professor Järvinen gave me the opportunity to work on this interesting project and has always provided me with excellent guidance and ideas concerning the research. During my time at the Institute, I have been a member of several research groups and it would be negligent of me not to acknowledge the help and support given by my former group leaders Doctors Kirsi Jylhä and Leif Backman as well as Professor Gerrit de Leeuw. I also am deeply grateful for my current group leader Doctor Heikki Lihavainen, who has always been helpful when I have sought his aid and who has allowed me a part of such a wonderful group.

My reviewers, Professors Markus Olin and Pertti Hari, provided valuable feedback which improved the thesis considerably. My many co-authors have improved the articles in this these by offering their invaluable expertise and patience. My colleagues both at the Finnish Meteorological Institute and at the University of Helsinki have always been ready to provide help with questions and created a truly enjoyable atmosphere to work in. For all of this I am filled with gratitude.

Finally, I must give thanks for my family and friends, without whom I would not be here. I cannot find the words to express how much I value them and thus must simply hope that they know it.

Estimating particle number size distributions from multi-instrument observations with Kalman filtering

Toni Tapani Viskari
University of Helsinki, 2012

Abstract

Atmospheric aerosol particles have several important effects on the environment and human society. The exact impact of aerosol particles is largely determined by their particle size distributions. However, no single instrument is able to measure the whole range of the particle size distribution. Estimating a particle size distribution from multiple simultaneous measurements remains a challenge in aerosol physical research. Current methods to combine different measurements require assumptions concerning the overlapping measurement ranges and have difficulties in accounting for measurement uncertainties.

In this thesis, Extended Kalman Filter (EKF) is presented as a promising method to estimate particle number size distributions from multiple simultaneous measurements. The particle number size distribution estimated by EKF includes information from prior particle number size distributions as propagated by a dynamical model and is based on the reliabilities of the applied information sources. Known physical processes and dynamically evolving error covariances constrain the estimate both over time and particle size.

The method was tested with measurements from Differential Mobility Particle Sizer (DMPS), Aerodynamic Particle Sizer (APS) and nephelometer. The particle number concentration was chosen as the state of interest. The initial EKF implementation presented here includes simplifications, yet the results are positive and the estimate successfully incorporated information from the chosen instruments. For particle sizes smaller than 4 μm, the estimate fits the available measurements and smooths the particle number size distribution over both time and particle diameter. The estimate has difficulties with particles larger than 4 μm due to issues with both measurements and the dynamical model in that particle size range. The EKF implementation appears to reduce the impact of measurement noise on the estimate, but has a delayed reaction to sudden large changes in size distribution.

Keywords: Atmospheric aerosols, Aerosol size distribution, Kalman Filters, Merging simultaneous observations

Contents

List of publications

This thesis consists of an introductory review, followed by 4 research articles. In the introductory part, these papers are cited according to their roman numerals. **Paper I** is reprinted under Elsevier's author rights. **Paper II** is reprinted under Taylor & Francis 's author rights. **Papers III** and **IV** are reproduced under the Commons Attribution 3.0 License.

I Viskari, T., Järvinen, H., Anttila, T., Kerminen, V.-M., Lehtinen, K. E. J., Korhonen, H., Sihto, S.-L. and Kulmala, M. (2008). Duration of the tangent-linear regime in sectional multi-component aerosol dynamics. *J. Aerosol Sci.*, 39:726-736

II Viskari, T., Kolmonen, P., Anttila, T. and Järvinen, H. (2010). The role of error covariances in estimation of aerosol number concentrations. *Aerosol Sci. Technol.*, 44(6):436-443

III Viskari, T., Asmi, E., Kolmonen, P., Vuollekoski, H., Petäjä, T. and Järvinen, H.(2012). Estimation of aerosol particle distributions with Kalman Filtering. Part I: Theory, general aspects and statistical validity. *Atmos. Chem. Phys. Disc.*, 12:18853-18887

IV Viskari, T., Asmi, E., Virkkula, A., Kolmonen, P., Petäjä, T. and Järvinen, H. (). Estimation of aerosol particle number distribution with Kalman Filtering. Part II: Simultaneous use of DMPS, APS and Nephelometer measurements. *Atmos. Chem. Phys. Disc.*, 12:18889-18925

1 Introduction

Aerosol is defined as a mixture of solid and/or liquid particles suspended in gas (Hinds, 1999), with aerosol size distributions representing how different aerosol variables are distributed over particle size. Individual aerosols affect radiation transfer, cloud formation and health in different ways. For example particles with diameters smaller than 1 μm generally scatter and absorb radiation in the visible light wavelengths more efficiently than particles larger than 1 μm. Aerosol size distributions thus directly affect visibility (Hand and Malm, 2007). The fraction of aerosol particles that act as cloud condensation nuclei increases with particle size. Aerosol size distributions are thus important with regard to cloud formation and nucleation (McFiggans et al., 2006). For atmospheric radiative transfer, aerosols have a direct effect, which refers to radiation scattering and absorption due to atmospheric aerosol size distributions, and an indirect effect, which refers to the role of aerosol size distributions in cloud formation (Myhre, 2009). Additionally, aerosols have several effects on health depending on particle size (Pope and Dockery, 2006). Due to these reasons, accurate characterization of aerosol size distributions is required to properly investigate and accurately understand the role of aerosol particles have in the atmosphere.

Atmospheric aerosols range several orders of magnitude in particle size and are composed of various chemical species in different internal and external mixtures. Currently it is impossible to measure all the properties of an aerosol size distribution with a single instrument (McMurry, 2000). Instead, different physical and chemical properties are measured by separate instruments, with the physical and chemical properties of aerosols and the particle number concentrations determined by post-processing the raw measurement data (e.g., Kandlikar and Ramachandran, 1999; Fiebig et al., 2005). These instruments can be divided to size-segregating detectors, which measure the size dependent aerosol quantities, and to integrating detectors, which measure quantities common for the whole aerosol size distribution. Combining measurements from different instruments into a single approximation of the aerosol size distribution has proven to be challenging and remains a relevant question even in current aerosol research. Several algorithms have been developed to determine an aerosol size distribution from independent measurement of different variables (e.g., Hand and Kreidenweis, 2002; Shen et al., 2002; Khlystov et al., 2010). These algorithms, however, usually require assumptions concerning both aerosol properties and the measurements themselves. In addition, they have difficulties accounting for the uncertainties of the measurements

and rarely guarantee a physically continuous system.

Data assimilation is a widely used mathematical method in geosciences to estimate system state from multi-instrument observations. Data assimilation methods produce a statistically optimal state estimates based on the available information sources. Data assimilation also includes information from states prior to the measurement time as evolved by the known physical processes. The state estimate will thus be constrained by both temporal continuity as well as the current physical understanding. Data assimilation has already been applied air quality (Elbern et al., 2001), environmental monitoring (Dubovik et al., 2008; Chung et al., 2010) and to improve aerosol mass, aerosol optical depth and extinction profile measurements (e.g., Liu et al., 2008; Tombette et al., 2009; Sekiyama et al., 2010; Schutgens et al., 2010) Here data assimilation is utilized to estimate a particle number size distribution from multiple in-situ measurements with a size segregated 0-dimensional aerosol microphysical model (a "box model").

The main objective of this thesis is to establish data assimilation, specifically Extended Kalman Filter (EKF), as a method to estimate a particle number size distribution from simultaneous multi-instrument observations which are generally continuous both over time and particle size. This objective is approached by

- Proving that the tangent-linear hypothesis required by the EKF implementation is valid for practical purposes **Paper I**
- Studying the error covariance structures created by an microphysical model and establishing the benefit of a dynamically evolving uncertainty regarding the state estimate **Paper II**
- Showing that EKF is capable of handling features typical for aerosol particle number size distributions and statistically comparing favorably EKF with a mathematical inversion method **Paper III**
- Estimating a variable state from multiple simultaneous in-situ measurements, which is reasonable in regard to all separate measurements **Paper IV**

2 Combining information from different detectors

2.1 Previous methods to combining information

Aerosol detectors rarely directly observe the state, but rather measure variables that are dependent on the state. The relation between the observations y and the state x can be assumed as

$$y = \tilde{g}(x), \tag{1}$$

where $\tilde{g}(x)$ is the relation between x and y. In reality $\tilde{g}(x)$ is not exactly known and all measurement contain measurement noise ξ. Thus eq. 1 expands to

$$y = g(x) + \xi, \tag{2}$$

where $g(x)$ is the known mathematical relation between x and y. In the case where $g(x)$ is sufficiently linear with respect to x, eq. 2 can be written as

$$y = \mathbf{G}x + \xi \tag{3}$$

where $\mathbf{G}$ is the linear form of $g(x)$. Solving x from eq. 3, if $\mathbf{G}$ is known, is referred to as a linear inverse problem. There are several mathematical methods to solve an inverse problem, which are detailed, e.g., in Voutilainen (2001).

Mathematical inversion is a generally efficient, easy-to-implement and computationally feasible method to produce a state approximation from a set of observations. There are also several different available methods to solve the inverse problem suitable for different situations and the solutions can be constrained by prior information. However, the mathematical inversion solution is a purely mathematical construct that does not inherently include physical information. It is also very difficult to separate ξ from x in the solution and the noise is projected over the solution by the possible smoothness constraints. Thus the accuracy of the solution is not known. Additionally, when the observations include multiple observations from same particle sizes, mathematical inversion methods can only produce a state approximate if the observations are directly

comparable and even then assumptions concerning the overlapping measurement range are necessary.

As mathematical inversion methods have difficulties approximating a state from multiple simultaneous observations, other methods have been used to combine observations from different detectors. In the context of the measurements used in this thesis, two methods are commonly used to approximate a combined state. Both require that the observations are first converted to functions of the same variable. The first option is to directly combine the separate parts of the available number concentration measurements by setting a cut-off diameter (e.g., Virkkula et al., 2011). The resulting particle number size distribution consists of measured number concentrations from different detectors on different sides of the cut-off diameter. Some measurements are always ignored beyond the cut-off diameter. The second option is to integrate different measurements using specific assumptions concerning particle properties based on experience, specific experiments determining those particle properties, or be obtained by optimization of the match between the instruments. This method can be used to combine different size-segregated measurements (Pitz et al., 2008) or determine appropriate parameters when comparing size-segregated and integrated measurements (Guyon et al., 2003; Virkkula et al., 2006; Petzold et al., 2009). Both of these solutions are practical, but do not properly account for measurement uncertainties or physical continuity of the state.

Next, Extended Kalman Filter is introduced as a method to estimate a particle number size distribution from multiple observations.

2.2 Extended Kalman Filter

All information concerning the value of a variable, i.e. variable state, contains uncertainty. Thus it is impossible to ever know the true state. Instead the state can be presented as a constrained probability density function (pdf), which is the likelihood for the true state based on existing information. At time step k, x_k is the state constrained by the preceding state x_{k-1} and model parameters θ according to

$$x_k \sim p(x|x_{k-1}, \theta) \tag{4}$$

$$\theta \sim p(\theta). \tag{5}$$

The pdfs are presented as p-functions. Here we assume a time-continuous system. As is seen in eq. 5, θ is also an approximation. The observations y_k are similarly constrained by the observable state according to

$$y_k \sim p(y_k|x_k). \tag{6}$$

If the uncertainties are gaussian and unbiased, then the pdfs in eqs. 4 and eq. 6 are normally distributed. In this case eqs. 4 and 6 can be written as

$$x_k = M(\bar{x}_{k-1}, \theta) + \epsilon_k \tag{7}$$

$$y_k = H(\bar{x}_k) + \omega_k, \tag{8}$$

where $\bar{x}_{k-1}$ and $\bar{x}_k$ are the expected values of x_{k-1} and x_k, respectively. The forward model M propagates the expected state to the next observation time and the observation operator H expresses how $\bar{x}_k$ would be observed. The model and measurement noise ϵ_k and ω_k, respectively, represent the deviations from the expected value.

The expected values in eqs. 7 and 8 are necessary for practical calculations. Determining ϵ_k and ω_k, however, would require non-erroneous information concerning the state, which will never be available. However, if the error is assumed to be Gaussian, it is possible to approximate the error variances $\sigma^2_{x,k}$ and $\sigma^2_{y,k}$ from eqs. 7 and 8. For state vector x_k and observation vector y_k, the uncertainties are presented in error covariance matrices $\mathbf{B}_k$ and $\mathbf{O}_k$, respectively. The diagonal values are the error variance terms and the non-diagonal terms represent the error interdependencies. Thus, it is possible to reasonably present both the state and the relevant accuracy.

Continuous-time filters consist of two alternating steps: i) time evolution and ii) observation updating. During the first step the state is propagated to the next observation time, where the second step composes a state estimate from the background state and observed state based on their reliabilities. The Extended Kalman Filter (EKF; Kalman

(1960); For textbook treatment, e.g., Kaipio and Somersalo (2004)) is a common mathematical filter application.

During the time evolution step, the previous state estimate $x_{a,k-1}$ is propagated to the observation time k. The propagated state x_k, also referred to as the background state as it contains information from the prior states, is determined according to

$$x_k = M(x_{a,k-1}). \tag{9}$$

Here the evolution model M can be non-linear. It is important to note that before the inclusion of the observations, x_k is the best available estimation of the state as it contains information from the prior observations as well as the known dynamical processes.

The background error covariance matrix $\mathbf{B}_k$ is calculated in a similar manner

$$\mathbf{B}_k = \mathbf{M}\mathbf{B}_{a,k-1}\mathbf{M}^T + \mathbf{Q}_k. \tag{10}$$

Here $\mathbf{M}$ is tangent-linear in respect to M. The term $\mathbf{M}\mathbf{B}_{a,k-1}\mathbf{M}^T$ describes the tangent-linear evolution of the state uncertainty. As uncertainty always spreads over time, $\mathbf{M}\mathbf{B}_{a,k-1}\mathbf{M}^T$ is larger than the initial $\mathbf{B}_{a,k-1}$. Error source term $\mathbf{Q}_k$ represents deficiencies in the model.

During observation updating, a new state estimate $x_{a,k}$ is composed by optimally weighing information from x_k and y_k according to

$$x_{a,k} = x_k + \mathbf{K}_k(y_k - Hx_k). \tag{11}$$

The difference between the observation and the background state counterpart is referred to as the innovation. The Kalman Gain $\mathbf{K}_k$ is determined by minimizing the variance of the state estimate and is

$$\mathbf{K}_k = \mathbf{B}_k\mathbf{H}^T[\mathbf{H}\mathbf{B}_k\mathbf{H}^T + \mathbf{O}_k]^{-1}, \tag{12}$$

where $\mathbf{H}$ is the tangent-linear version of H. The impact of the innovation on the state estimate is based on the relative uncertainties of the different information sources. The more reliable the observations are in comparison with respect to the background state, the more the innovation will affect the state estimate. In case there are multiple observations of the same state, then their combined impact on the state estimate is determined by calculating the weighed mean of the innovations. The weight of each innovation is determined by the respective relative uncertainty.

The error covariance matrix for $x_{a,k}$ is simultaneously estimated with

$$\mathbf{B}_{a,k} = [\mathbf{I} - \mathbf{H}^T \mathbf{K}_k]\mathbf{B}_k, \tag{13}$$

which is the minimal variance calculated when solving $\mathbf{K}_k$. The observation update will thus always produce a statistically more reliable state estimate than any of the individual information sources used during observation update.

The EKF process is summarized in Fig. 1. In essence, EKF corrects the time-evolved state according to recent observations. The comparative accuracy of the observations and background state determines the weight given to the information sources. It is important to note that EKF does not directly combine the different observations and uncertainties. Instead it updates the background state according to the available observations and their uncertainties.

The variable of interest in this study is the particle number size distribution. Application of EKF requires the following: i) A reliable mathematical forward model, ii) Observations relating to the particle number concentration, iii) Observation operators and iv) The error covariance matrices.

2.3 The forward model

The forward model evolves the state from one observation time to the next in order to determine the background state. In this research, University of Helsinki Multicomponent Aerosol model (UHMA; Korhonen et al., 2004) was used as the forward model. UHMA is a size-segregating box model, which depicts the major microphysical processes evolving the particle size distribution. There are several UHMA versions for

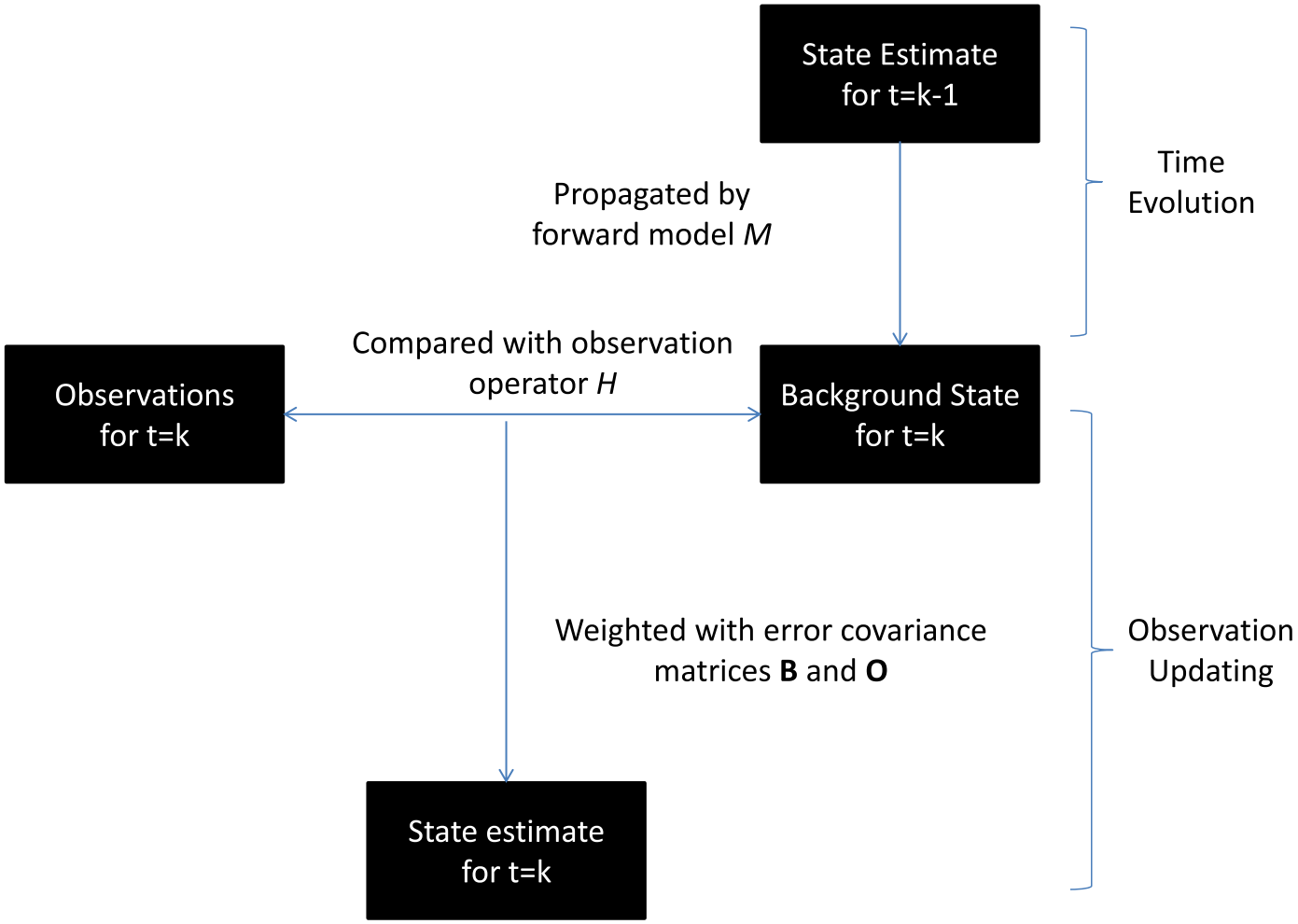

Figure 1: The EKF process

different conditions. A basic model including nucleation, condensation, coagulation and dry deposition processes was used as the forward model here.

During the nucleation process, new particles are formed from ambient vapours. Here the nucleation rate J is determined by the activation scheme (Sihto et al., 2006; Kulmala et al., 2006)

$$J = A[\mathrm{H_2SO_4}], \tag{14}$$

where A is the activation coefficient and $\mathrm{H_2SO_4}$ is the ambient sulphuric acid vapour concentration. The formation of new particles is thus directly dependent on the ambient sulphuric acid concentration. The new particles are always formed in the lowest model size bin. The activation coefficient was set as $3 * 10^{-6} \frac{1}{s}$.

During the condensation process, ambient vapour condenses on the particle surfaces. The evaporation of compounds from the particle surface is here also included in the condensation process. The condensation rate $I_{v,a}$, which represents the change in particle volume V due to compound a is determined with

$$I_{v,a}(V) = \frac{2\pi^{\frac{2}{3}}(6V)^{\frac{1}{3}} D_{v,a} M_a}{\rho_a R_g T} f(Kn, a) f_p(p_\alpha - p_{sat,a}), \tag{15}$$

where M_a is the molecular mass of the compound a, R_g is the gas constant, ρ_a is the density of the compound, T is the temperature and $D_{V,a}$ is the diffusion constant for the vapour. Function $f(Kn, a)$ is the correction term for calculation assumptions. Function f_p describes how the difference between the partial gas vapour pressure p_a and saturation vapour pressure $p_{sat,a}$ for a affects $I_{v,a}$. The adjusted Fuchs-Sutugin method (Fuchs and Sutugin, 1971; Lehtinen and Kulmala, 2003) was used here to determine $I_{v,a}$. For organic compounds, the nano-Köhler theory (Kulmala et al., 2004) has been included. The condensation process conserves the total number concentration, only affecting the particle number size distribution by changing particle diameters.

During the coagulation process, particles collide together forming a new particle that has the combined dry volume of the two colliding particles. The collision rate $J_{i,j}$ between particle diameter d_i and d_j is calculated with

$$J_{i,j} = K_{i,j} N_i N_j, \tag{16}$$

where N_i and N_j are the number concentrations in the respective particle sizes. The coagulation kernel $K^k_{i,j}$ was taken from Fuchs (1964). The coagulation process always reduces the total number concentration of a size distribution.

During the dry deposition process, particles are removed from the air mass to surrounding surfaces due to gravity or air flow. The dry deposition flux is calculated with

$$F^d_i = -v_d N_i, \tag{17}$$

where F_i is the deposition flux for particle size d_i. The deposition velocity v_d was determined according to Rannik et al. (2003) and extrapolated to particle sizes smaller than 10 nm. Wet deposition, was not included in this UHMA version. The dry deposition always decreases the total number concentration.

Here, UHMA calculates the processes in the following order. First, the nucleation process determines the influx of new particles. Second, the condensation process evolves the particle number size distribution. Finally, both the coagulation and deposition processes are concurrently calculated from the same size distribution. Particles are assumed to be composed of the same compounds than those used as ambient vapours. In these experiments, the model has 60 logarithmically evenly spaced size bins. The smallest (largest) particle size is 1.5 nm (20 μm).

As explained in Section 3.2, EKF requires a tangent-linear version of UHMA. The tangent-linear version of an operator is the gradient in the first order term of the Taylor expansion of the operator. As long as the first order term dominates the Taylor expansion, it is possible to approximate the uncertainty propagation according to the tangent-linear hypothesis. The construction of the tangent-linear version of UHMA is detailed in **Paper I**. In the same article the tangent-linear version of UHMA is found to be valid for time intervals shorter than 30 minutes.

2.4 Detectors and observation operators

To properly assess the effectiveness of EKF regarding aerosol physics, observations are from four separate instruments and three different observable quantities are included in the EKF implementation. These instruments include two Differential Mobility Particle Sizers, which have different measurement ranges, an Aerosol Particle Sizer and a nephelometer.

As these instruments measure different quantities over different particle size ranges, an observation operator, as presented in eq. 8, is required to compare the observations to background state calculated by the forward operator. The instrument-specific observation operator presents how the respective instrument would observe the background number size distribution. By projecting the background state to the different particle size ranges as values of the relevant measurable quantities, the observation operators make it possible to determine the differences between the background and observed states. Thus the observation operator allows incorporating information from very different measurement instruments and is necessary for the observation updating. A tangent-linear version of observation operator is also needed by EKF as seen in eq. 12.

In the following subsections first the detector is explained and then relevant observation operator is introduced.

2.4.1 Differential Mobility Particle Sizer (DMPS)

Differential Mobility Particle Sizer (DMPS; Hoppel, 1978) is a size-segregating detector that measures particle number concentrations as a function of voltage. The theoretical basis for DMPS is that the velocity v_{TE} of a particle in electrical field E is given by

$$v_{TE} = ZE, \tag{18}$$

where Z is the electrical mobility. Electrical field is created by a set voltage and v_{TE} can be calculated from the distance the particle travels during a specific time. Assuming that the flow is not turbulent, Z can be written as

$$Z = \frac{v_{TE}}{E} = \frac{neC_c}{3\pi\eta d}, \tag{19}$$

where e is a single charge, n the number of charges carried by the particle, C_c is the slip correction function, η is the gas viscosity and d is the Stokes diameter of a particle. From eq. 19, d can be solved.

The DMPS instrument is composed of three separate parts. Neutralizer forces the particle number size distribution to a steady-state charge distribution. Differential Mobility Analyzer (DMA) creates an electrical field perpendicular to a flow field. The electrical field moves the particles towards the electrode while the flow field moves the particle parallel to the electrode. As the velocity of the flow field is known as well as the distance of the electrode from the DMA inlet, v_{TE} can be approximated. Measurements are classified according to voltage which causes the electrical field. Properly set DMA is able to measure particles with diameters smaller than 10 nm, which are too small to be optically measured. The Condensation Particle Counter (CPC; McMurry, 2000) determines the number concentration for the separated particles by condensing vapour on the particles until they are large enough to be optically detected.

Converting particle number concentrations as a function of voltage as measured by DMPS to particle number concentration as a function diameter requires accounting for several aspects of measurement instrument. Not all particles are charged in the neutralizer and especially large particles can carry more than one charge. Thus it is necessary to approximate the charging probability for different particle sizes (Wiedensohler, 1988). The number of particles measured for by DMA for a single voltage, referred to as the measurement channel, is a function of particle diameter and triangular in shape. Transfer functions for measurement channels express how the measured particle number concentration is distributed over adjacent particle sizes (Stolzenburg, 1988). Finally, particle size dependent losses during the measurement process must be accounted for (Aalto et al., 2001).

Here the DMPS observations are from a Twin-DMPS system, where two DMPS:s concurrently measure different particle sizes. The smallest, 3 to 40 nm, particles were measured using a DMPS consisting of a 10.9 cm long Vienna type DMA (Winklmayr et al., 1991) and a TSI CPC model 3025 (Stolzenburg and McMurry, 1991). The bigger, 10-1000 nm particles, were measured using a DMPS consisting of a 28 cm long Vienna type DMA and a TSI CPC model 3010 (e.g., Quant et al., 1992). The Twin-DMPS

has an overlapping measurement region of 10-40 nm. Each DMA channel is measured subsequently with a 10 minute measurement cycle, but here it is assumed that the all measurements are from the same time. In reality the particle number size distribution evolves constantly over the measurement cycle. An 85-krypton bipolar neutralizer was used as the neutralizer for both DMPS:s. The charging probabilities were determined according to Wiedensohler (1988). The measurement system is more thoroughly explained in Aalto et al. (2001). Here both DMPS:s are treated as individual detectors for the EKF implementation. The DMPS measurements deployed here are a part of the EUSAAR network, thereby following the network quality standards presented in Wiedensohler et al. (2010).

The observation operator for DMPS, H_{DMPS}, is the product of two matrices

$$H_{DMPS} = \mathbf{RP}. \tag{20}$$

The DMPS interpolation matrix $\mathbf{P}$ calculates the model output at the characteristic diameters of the DMPS instrument from the background state. The instrument kernel matrix $\mathbf{R}$ determines the number concentrations for the measurement channels from the interpolated number concentrations. The kernel matrix was assumed to be constant in time.

A cumulative distribution function (CDF) is used to determine $\mathbf{P}$. First, the CDF value for a model diameter is computed by summing up the number concentrations for all smaller model diameters. 4^{th} order Lagrange polynomials are then used to interpolate the CDF values from the model grid to the instrument grid. Finally, particle number concentrations for the instrument grid are gained by subtracting consecutive CDF values from each other. All the numerical operations required for H_{DMPS} are linear and thus a separate tangent-linear version is unnecessary.

2.4.2 Aerodynamic Particle Sizer (APS)

The Aerodynamic Particle Sizer (APS) is a size-segregating detector that measures particle number concentrations as a function of aerodynamic size. The instrument classifies particles based on how long it takes them to pass two concurrent lasers in an accelerated flow field. This is based on Stokes's law, which states that the settling velocity v_{TS} in a gas flow is (Hinds, 1999)

$$v_{TS} = \sqrt{C_c(d_p)}\frac{\rho_p d_p^2 g}{18\eta\chi} = \sqrt{C_c(d_a)}\frac{\rho_0 d_a^2 g}{18\eta}, \tag{21}$$

where d_p and d_a are equivalent and aerodynamic particle diameters, respectively, g is the gravitational acceleration, C_c is again the slip correction factor, χ is the dynamic shape factor and ρ_p and ρ_0 are the densities for the particle and water, respectively. As it is generally impossible to know the composition and shape of each measured particle, the APS measurements are always given as a function of d_a, which is the diameter of a spherical particle composed of water. From eq. 21, d_p can be written as a function of d_a

$$d_p = d_a\sqrt{\frac{C_c d_a}{C_c(d_p)}}\sqrt{\frac{\rho_0\chi}{\rho_p}}. \tag{22}$$

It is important to note that d_p is the equivalent diameter of a possibly non-spherical particle, while d used in eq. 19 is the diameter for a spherical particle.

Here TSI model APS 3321 (Peters and Leith, 2003) was used to measure particles with diameters between 0.5 and 20 μm. Inlet line losses in measurements are minimized with vertically positioned moderately heated inlet. With properly calibrated inlet- and aerosol flow rates, the aerodynamic sizing of the APS can be considered accurate. A large uncertainty is expected for the concentration, mainly due to the losses inside the instrument and the inlet tubes. The instrument losses have been shown to depend on particle size and aerosol phase (Volckens and Peters, 2005) and are thus not easy to correct accurately. When concentration is high, additional uncertainty may arise from particle collision within the detection time.

The observation operator for APS, H_{APS}, is determined in two steps. First, the equivalent diameters are calculated from the aerodynamic diameters with eq. 22. Few assumptions were made during this step. The slip correction function Cc is nearly constant for particles larger than 700 nm and thus the relation $C_c(d_a)/C_c(d_p)$ is approximated as one. The aerosol particles were assumed to be spherical, for which χ is one. These approximations reduce eq. 22 to

$$d_p = d_a\sqrt{\frac{\rho_0}{\rho_p}}. \tag{23}$$

Particle density changes both over time and particle size, but here it assumed to be constant. Based on Saarikoski et al. (2005) and Kannosto et al. (2008), ρ_p is approximated as 1.5 g/cm^3. Second, the measurement grid diameters have been calculated, the background state is interpolated to them from the model grid.

2.4.3 Nephelometer

Nephelometer (Beuttell and Brewer, 1949; Ahlquist and Charlson, 1967; Bodhaine et al., 1991) is an integrating detector that measures radiation scattering from an air mass. As radiation passes through air, fraction of the radiation changes direction due to interference from particles and molecules present in the air. This direction deviation is defined as total radiation scattering. The part of the radiation which is reflected back to the direction from which the original radiation came from is defined as radiation backscatter. The focus here is on the total radiation scattering. Radiation scattering S for wavelength λ as measured by the nephelometer can be written as

$$S(\lambda) = \int_{0^\circ}^{180^\circ} F(\lambda, \Theta) z(\Theta) \delta\Theta, \tag{24}$$

where Θ is the inclination angle of the radiation scattering, z is the angular sensitivity function for the nephelometer and the angular scattering function F(λ,Θ)

$$F(\lambda, \Theta) = \int_{-\infty}^{\infty} f_\lambda(\Theta, d, m) \frac{\pi d^2}{4} \frac{\delta N(d)}{\delta \log d} \delta \log d + F_R(\Delta). \tag{25}$$

Here $N(d)$ is the number concentration as a function of d, f_λ is the angular scattering function for individual particles and $F_R(\Delta)$ radiation scattering due to carrier gas molecules. The complex refractive index $m = m_r + im_i$ represents both radiation refraction m_r and radiation absorbtion m_i. For an ideal nephelometer

$$Z(\Theta) = sin\Theta. \tag{26}$$

Taking into account the calibration constant $K_c(\lambda)$ and Rayleigh scattering coefficient for the gas $\varphi_R(\lambda)$, scattering coefficient $\varphi_{SP}(\lambda)$ is determined by

$$\varphi_{SP}(\lambda) = K_c(\lambda)S(\lambda) - \varphi_R. \tag{27}$$

Rayleigh scattering $\varphi_R(\lambda)$ can be calculated analytically (e.g. Buchholz (1995)), if temperature and pressure are known. After integrating S over Θ, eq. 27 becomes

$$\varphi_{SP}(\lambda) = \int_{-\infty}^{\infty} Q_{SP}(\lambda, d, m)\frac{\pi d^2}{4}\frac{\delta N(d)}{\delta \log d}\delta \log d. \tag{28}$$

The scattering efficiencies Q_{sp} were calculated using the Mie scattering of Barber and Hill (1990).

Equation 28 contains two important assumptions. First, in eq. 26 it was assumed that the radiation was formed from Lambert radiation emission, i.e. that z can be approximated as a sine-function. This causes a small deviation in the measurements (Anderson et al., 1996). Secondly, the nephelometer measurements are over a limited angular integration range (Moosmüller and Arnott, 2003) instead over the 180∘ assumed in eq. 24. When correcting the measurements concerning these limitations, it is important to note that both the particle scattering as well as the carrier gas scattering are affected. The measurements are corrected by first calculating Ångström exponents from the non-corrected scattering coefficients and then according to the formulas shown in Anderson and Ogren (1998).

A detailed description of the aerosol optical measurements is given in Virkkula et al. (2011). Air measured with aerosol optics instruments was sampled through a PM10 inlet. The sample is dried before entering the instruments. Scattering coefficients at wavelengths of 450, 550 and 700 nm were measured with a TSI 3λ nephelometer (Anderson et al., 1996). The instrument measured radiation scattering by emitting light to the examined air mass and employing a light-detector set to one-side of the light source. The measurements were averaged over a 5 minute interval. The EKF implementation only uses scattering coefficient measurements which are approximately from the same nominal time than the DMPS and APS measurements. The pressure and temperature of the nephelometer was also measured in order to correct the scattering coefficient to 1000 mbar and 0°C.

For the observation operator H_{neph}, eq. 28 was assumed to be a sum over discretized particle sizes. The observation operator contains $Q_S P$ values for all particle sizes in the

model grid. The refractive index m changes over time and particle diameter. Here it was simplified by setting m_r and m_i to constant values of 1.517 and 0.005, respectively, based on Virkkula et al. (2011).

2.5 Error covariance matrices

The error covariance matrices have two purposes in EKF. Error variances represent the reliability of the information source, which is necessary to properly weigh the information. For example if the observations are more reliable than the background state, then in eq. 11 the state estimate is closer to the observed state than the background state. The error covariances in turn represent the linear connections between uncertainties of different variables, or specifically in this implementation, different particle sizes. Thus the error covariances spread information from a single measurement over the whole particle number size distribution. Here, it was necessary to simplify both the observation and background error covariance matrices.

The observation error covariance $\mathbf{O}_k$ contains the measurement uncertainties for all the included instruments. Three different factors determine $\mathbf{O}_k$: I) The instrument error which represents the inherent uncertainty of the detector, i.e. the observation noise, II) Observation operator error which describes the observation operator's limited capability to reproduce the instrument response to the background state, and III) Representation error reflects the background state not including all the dynamical processes affecting the size distribution. All these components interact and thus it is not possible to approximate $\mathbf{O}_k$ from a single error component alone. Currently it is possible to approximate the instrument error prior to the EKF implementation, but the observation operator and representation errors require statistical information gained from EKF.

Here $\mathbf{O}_k$ is assumed to be diagonal, i.e. different measurement channels are independent of each other. The error standard deviations are assumed to be instrument-specific values relative to the measured number concentration. The set relative error is 15% for DMPS I and APS, and 12% for DMPS II (Personal communication, Pasi Aalto,2012). The three lowest APS measurement channels is an exception here, as the measurements from them are clearly erroneous. To mitigate the impact of these observations, the relative error for the three lowest APS measurements channels is set to 45%. For nephelometer, the relative error is set as 7% (Heintzenberg et al., 2006). The error is

here larger for DMPS I and APS than for DMPS II as the measurement noise has more impact on small number concentration measurement values. In this initial application, observation error for an instrument is not size dependent.

In **Paper II**, it was shown that a dynamically evolving $\mathbf{B}_k$ benefits the state estimate. As seen in eq. 10, the background error covariance matrix $\mathbf{B}_k$ is composed of evolved previous state estimate error and the model error $\mathbf{Q}_k$. Here, there are two major challenges in determining $\mathbf{B}_k$. First, there are currently no methods to determine $\mathbf{Q}_k$ and thus it cannot be included in $\mathbf{B}_k$ here. This is especially a problem for UHMA as it includes several approximations and parameterization that are not always valid. Second, uncertainty increases during the state propagation and decreases during the observation update as seen in eq. 13. If the uncertainty increases too slowly during state propagation, then the state estimate error will be consistently smaller after each observation update. This decrease ultimately leads to $\mathbf{B}_k$ becoming much smaller than $\mathbf{O}_k$, which causes to the observation updating to effectivlely ignore the observation information. In data assimilation this is known as filter divergence.

In order to avoid filter divergence, $\mathbf{B}_k$ was simplified. Background state error variances are scaled so that the relative error for any particle size in the measurement range cannot be smaller than 20%. The background error covariances are simultaneously corrected so that the error correlations remain constant in the scaling. This ensures that the observations will always have more weight during the observation update step.

In **Paper II** it was established that UHMA creates a strong correlation between particles smaller 10 nm and particle sizes where condensation sink (Kulmala et al., 2001) is the largest. This correlation can cause the EKF implementation to become unstable, if there is a large difference between the background and observed state. To avoid this instability, the background error covariance matrix was restricted so that a large innovation affects the size distribution at the maximum distance of 20 size bins of the UHMA model.

3 Results and analysis

In **Paper III** and **Paper IV**, the EKF implementation was tested with observations from SMEAR II (Station for Measuring Ecosystem/Atmosphere Relations) measurement station in Hyytiälä, South-Western Finland (61°47”N, 24°42”E, 181 m AMSL)

(Hari and Kulmala, 2005). All the figures in this section are from those two papers. The specific measurements used here are from April-May 2007 and were made as a part of the EUCAARI project (Kulmala et al., 2009). As mentioned in Section 3.4, the included measurements are from a Twin-DMPS, an APS and a nephelometer instruments. Ambient sulphuric acid and non-volatile organic vapour concentration measurements (Petäjä et al., 2009; Paasonen et al., 2010) were utilized in UHMA simulations. Ambient concentrations for a volatile organic vapour were estimated from the non-volatile organic vapour concentrations according to Vuollekoski et al. (2010). The ambient vapour concentrations are linearly interpolated for 10 second time intervals and used as the ambient vapour concentrations values in the UHMA model. The vapour profiles are presented in Fig. 2. Ambient atmospheric conditions (temperature, etc.) were specified as constants due to the model being not particularly sensitive to these values.

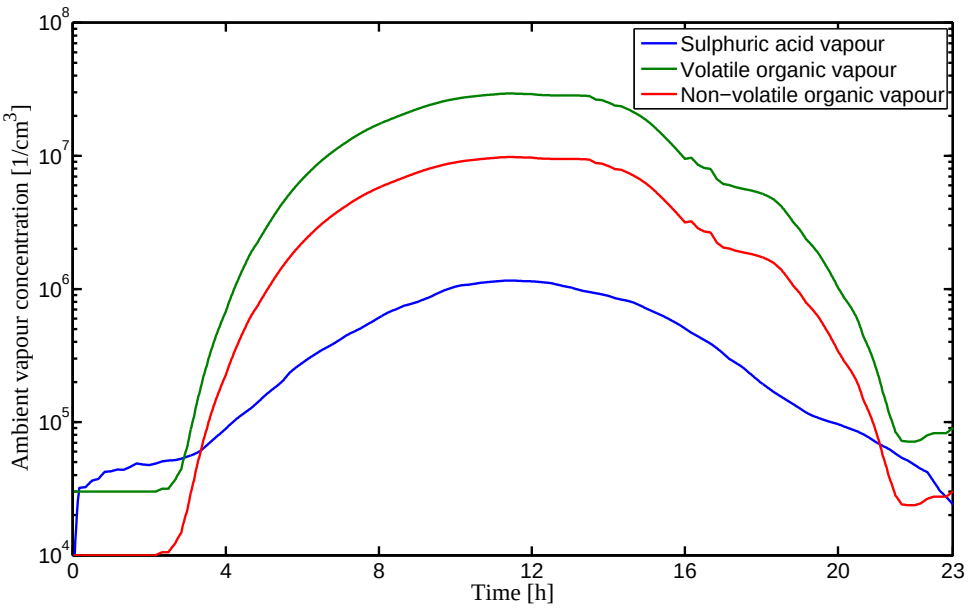

Figure 2: The ambient vapour concentrations for sulphuric acid (blue), non-volatile organic compound (red) and volatile organic compound (green) as applied in the EKF implementation for 7 May 2007.

The results presented here are for 7 May 2007, which was chosen because during this day the particle number size distribution notably evolves in different ways, e.g. due to a strong nucleation event and to a sudden change in the size distributions. The results for this day were found to be well-representative for the rest of the studied period.

As mentioned in Section 2.4, both particle density ρ and refraction index m were assumed constant in this initial EKF implementation. This is not reflective of actual measurement conditions, where both parameters change over particle size and time. In order to study the impact of this simplification, the simulations were repeated with separately perturbed parameter values (by 0.2 g/cm^3 for ρ, 0.1 units for m_r and 0.01 units for m_i; results not shown). The perturbed parameter values did have a noticeable effect on the state estimates, but the resulting state estimate remained similar to those presented here. In addition, the measurements and their associated uncertainties had a far larger impact on the state estimate. Thus here the focus is solely on the measurements. However, the constant parameterizations will be addressed in future work.

The state estimate should be compared to other particle number size distributions combined from multi-instrument observations. Here a combined particle number size distribution is combined by using the Twin-DMPS inverse solution up to particle diameter of 700 nm and continuing APS measurements after that. The geometric diameters were calculated for the APS measurements. The inverse solution for DMPS measurements is found with a least-square nonnegative pseudo-inverse method where the observations in the overlapping region are averaged from the two information sources. The combined size distribution is then interpolated to a logarithmically evenly spaced grid, which had 74 size bins. The smallest (largest) particle diameter in the new grid is 3.5 nm (15 μm).

Particle size number distribution estimated by EKF with DMPS and APS measurements is referred to as x^N_{DA}, particle size number distribution estimated by EKF with DMPS, APS and nephelometer measurements as x^N_{DAN}, and the reference particle size number distribution combined from DMPS and APS measurements as x^N_{com}. The estimated size distribution (x^N_{DAN}; Fig. 3a) and the combined size distribution (x^N_{com}; Fig. 3b) are shown from 00:00 to 23:00 Local Time (LT) for 7 May 2007. All the diameters are defined as the Stokes diameter of the particle (Hinds, 1999). Note that the results are given in different resolutions. In both x^N_{DAN} and x^N_{com} a strong nucleation event is visible after approximately 10:00 LT and there are sudden changes in particle num-

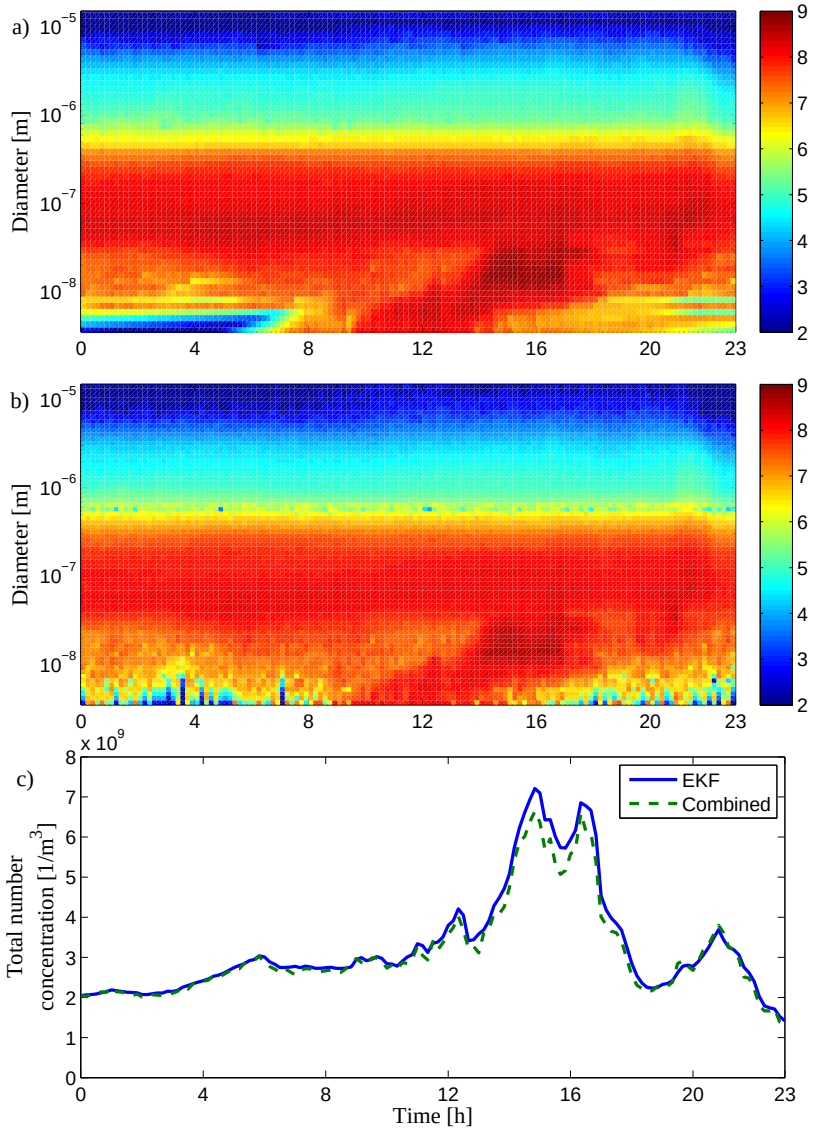

Figure 3: a) Particle number size distribution obtained with EKF using DMPS and APS observations (x^N_{DAN}) on 7 May 2007 from SMEAR II in Hyytiälä, Finland. Note that the particle number concentrations are only presented from 10^2 to 10^9 1/m^3. The color bar values are given as exponents of 10. b) As in a), but for x^N_{com}. c) The total number concentrations for particles larger than 3 nm for (x^N_{DAN}) (blue, solid) and (x^N_{com}) (green, dashed)

ber concentrations after 17:00 and 21:00 LT. The size distributions are similar overall, although x^N_{DAN} is smoother over subsequent measurement times and more continuous over particle diameter than x^N_{com}, especially in particle sizes smaller than 20 nm and in diameter range of 500-1000 nm. The total number concentration for x^N_{DAN} and x^N_{com} are shown in Fig 3c. The total number concentrations follow each other closely with the total number concentration for x^N_{DAN} having slightly larger values. The differences in the total number concentrations are partially due to the diameters for x^N_{DAN} and x^N_{com} not being the same, which makes it difficult to limit x^N_{DAN} to the same diameter range than x^N_{com}. At approximately 15:00 and 17:00 LT, the total volume concentration is much larger for x^N_{DAN} than for x^N_{com}.

Figure 3 demonstrates that the EKF implementation reduces the impact of apparently random variations in the number concentration measurements by including prior information from the background state and constraints due to error covariances. During the sudden changes at approximately 17:00 and 21:00 LT, the background state contradicts the observed state, which causes x^N_{DAN} to have a delayed adjustment to the measured state. This is especially visible as a difference between total number concentrations in Fig. 3c after approximately 17:00 LT and also after 21:00 LT, where in both cases it takes 2-3 measurement cycles, specifically 20-30 minutes, for x^N_{DAN} to re-adjust to the new measurement state. The large difference between the total number concentrations after 15:00 LT is due to x^N_{com} drastically underestimating the particle number concentrations in particle sizes smaller than 20 nm.

Both particle number size distribution and total number concentration are dominated by particles smaller than 300 nm, as is seen in Fig. 3. Number concentrations measured by APS, though, are for particles larger than 400 nm, and nephelometer measurements are most sensitive for number concentrations in the particle size range of 300-700 nm. To better illustrate how APS and nephelometer measurements affect the state estimate, particle volume size distribution, which is the sum of particle volume within a size bin and which is dominated by particles larger than 100 nm, is presented in Fig. 4. The volume concentration for x^N_{DA} will be referred to as x^V_{DA} (Not shown), for x^N_{DAN} as x^V_{DAN} (Fig. 4a) and for x^N_{com} as x^V_{com} (Fig. 4b). Note that the volume of a particle increases with particle diameter, causing the differences between x^N_{DAN} and x^N_{com} result in larger differences between x^V_{DAN} and x^V_{com}. As in Fig. 3, the particle volume size distributions resemble each other, with x^V_{DAN} being more continuous over the overlapping measurement range of 0.4-1 μm and smoother over time than x^V_{com}.

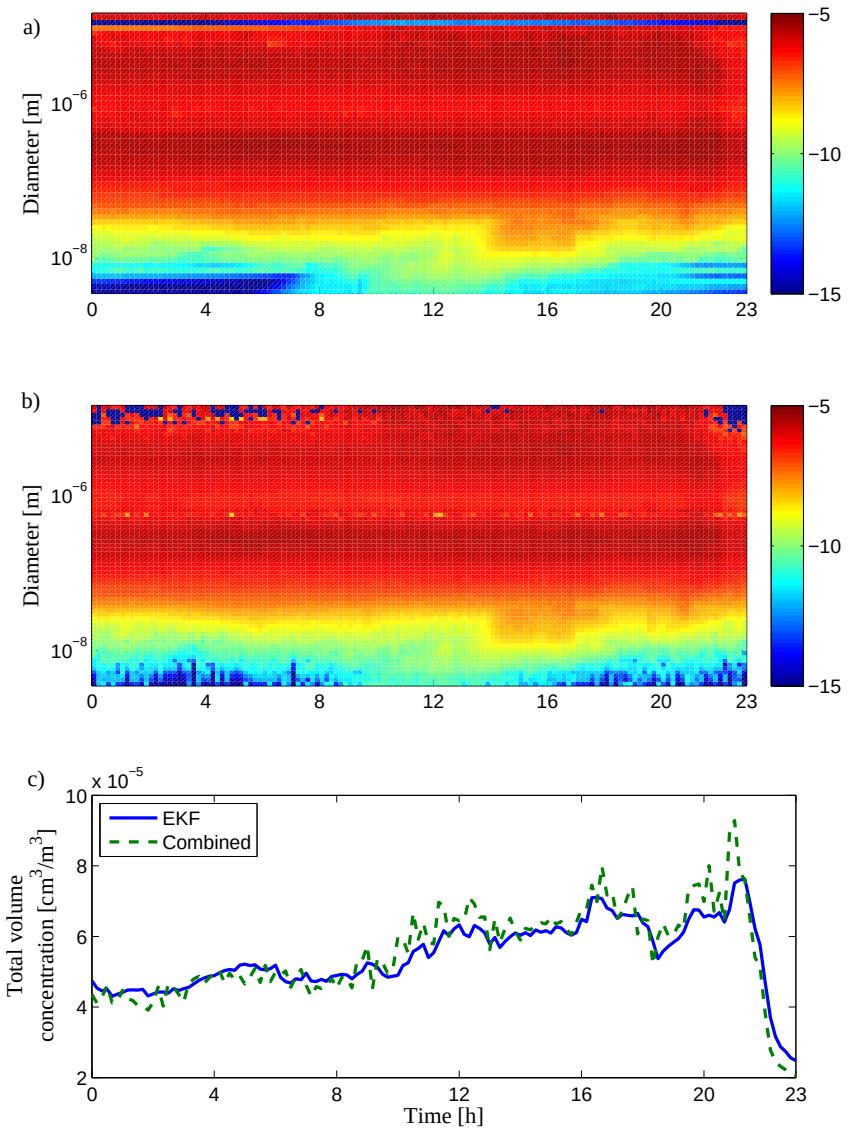

Figure 4: a) Particle number size distribution obtained with EKF using DMPS and APS observations (x^N_{DAN}) on 7 May 2007 from SMEAR II in Hyytiälä, Finland. Note that the particle number concentrations are only presented from 10^2 to 10^9 $1/m^3$. The color bar values are given as exponents of 10. b) As in a), but for x^N_{com}. c) The total number concentrations for particles larger than 3 nm for (x^N_{DAN}) (blue, solid) and (x^N_{com}) (green, dashed)

However for particles larger than 10 μm, x^V_{DAN} and x^V_{com} differ greatly. For x^V_{DAN}, the particle volume concentration decreases drastically near particle sizes 10 μm and then increases again for particles larger than 13 μm. For x^V_{com}, instead, the particle volume concentration evolves erratically in those particle sizes and especially after 08:00 LT it is very different from x^V_{DAN} in those particle sizes. The total volume concentrations for both size distributions over time are presented in Fig. 4c. They follow each other closely, but the total volume concentration for x^V_{com} varies more over time than the total number concentration for x^V_{com}.

The EKF implementation appears to successfully produce a state estimate from simultaneous measurements which is continuous over both particle size as well as time and is consistent with the separate measurements. To illustrate this, both x^V_{DAN} and its corresponding values in the DMPS II and APS measurement channels according to H as well as for the actual measurements over particle sizes 30 nm - 10 μm at 12:00 LT are presented in Fig. 5. The state estimate follows the measured values of both DMPS II and APS for particles smaller than 4 μm. For particles larger than 4 μm, though, the measurements become discontinuous over particle diameter and the state estimate differs from the measured values. Comparison between total number concentration for x^N_{com} (Fig. 3c) and total volume concentration for x^V_{com} (Fig. 4c) show that the total volume concentration varies more over subsequent measurement times than the total number concentrations. The measurement noise thus has a larger impact in particle sizes larger than 400 nm as the number concentrations in those particle sizes dominate the total volume concentrations. This interpretation is supported by Volckens and Peters (2005), which stated that the APS measurement accuracy decreases with increasing particle size.

The differences between x^V_{DAN} and x^V_{com} for particles larger than 4 μm are partially due to apparently random evolution of the observed particle number size distribution in those particle sizes. There are, however, other difficulties for the EKF implementation in this size region. State estimates are constrained over particle diameter by the aerosol dynamical processes, whose impact on the particle number size distribution is reduced as the particle diameter increases. For particles larger than 4 μm, the error covariances are very weak and thus are only a minimal constraint for the state estimate. In addition, UHMA does not predict the increase of measured particles larger than 4 μm after 08:00 LT visible in Fig. 4b. The challenges for the EKF implementation in this size range are thus due to both the measurements and model limitations.

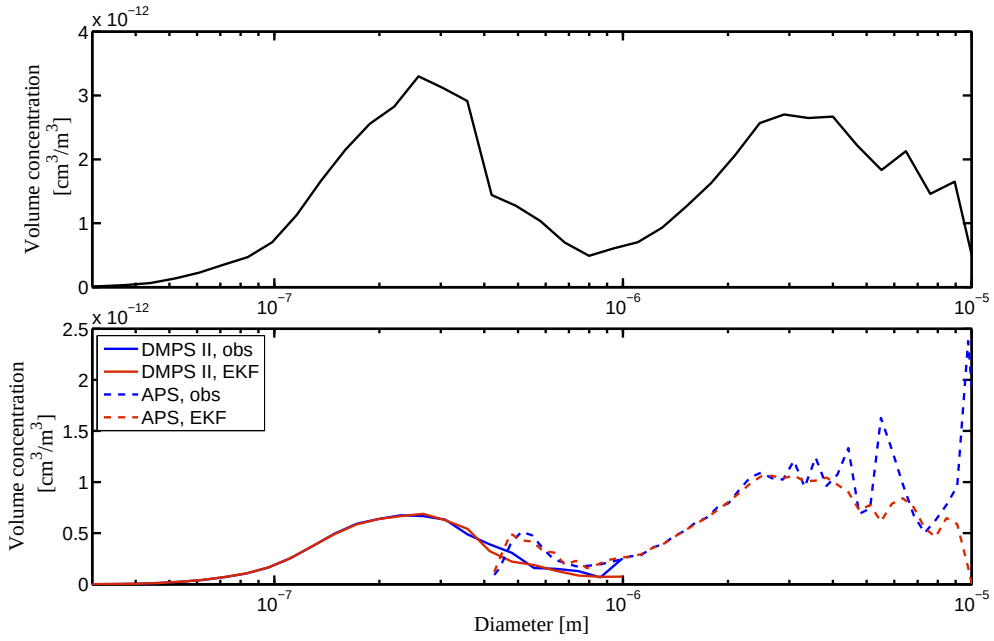

Figure 5: The estimated volume concentration size distribution in 300 nm -2 μm at 12:00 7 May 2010 from SMEAR II in Hyytiälä, Finland (top panel). The observations (blue) and corresponding estimate calculated with H (red) from 300 nm to 2 μ for DMPS II (solid) and APS (dashed) from 12:00 on 7 May 2010 from SMEAR II in Hyytiälä, Finland (bottom panel).

The impact of integrating measurements on the state estimate depends on how different particle sizes affect the observed value. The nephelometer measures electromagnetic radiation scattering in the visible wavelength, which is dominated by particles in the size range of 300-700 nm. Consequently, in the EKF implementation, the nephelometer observations primarily affect this size range and have only a limited impact on other particle sizes. The nephelometer measurements generally affect the state estimate less than DMPS or APS measurements. Instead, the nephelometer measurements reduce the impact of DMPS and APS measurement noise on the state estimate and provide supporting information when the size-segregating measurements disagree with each other or with the background state. The role of the nephelometer observations is most prominent at approximately 21:00 LT in Fig 4, when x^V_{com} shows a large change in particle number size distribution that is visible in x^V_{DAN} roughly 20 minutes later. This difference between x^V_{DAN} and x^V_{com} is due to DMPS and APS observing the sudden

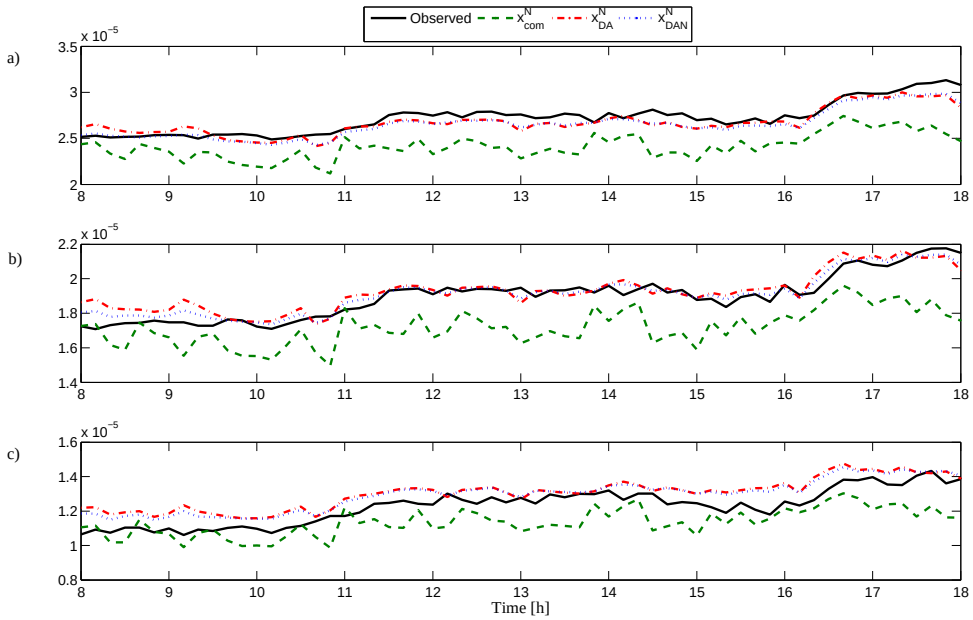

Figure 6: The observed scattering (φ_{obs}; black, solid), the scattering calculated from x^N_{DA} ((φ_{DA}; red, dot-dashed), from x^N_{DAN} ((φ_{DAN}; blue, dotted) and from x^N_{com} ((φ_{com}; green, dashed) for wavelengths 450, 550 and 700 nm (a, b and c respectively)

change in air mass at approximately 21:00 LT and the nephelometer measuring a sudden change in scattering coefficients after 21:20 LT. x^V_{DAN} reaction to the sudden change is slowed by these contradicting observations, with x^V_{DA} having a faster reaction to the sudden change (Not shown). This difference in reaction demonstrates both the effect integrating observations can have on the state estimate and why synchronization of detectors is important for EKF.

The measured and calculated scattering coefficients for 08:00-18:00 LT for 7 May 2007 for wavelengths 450, 550 and 700 nm are presented in Fig. 6. The measured scattering coefficients are referred to as φ_{obs}, scattering coefficients calculated from x^N_{DA} as φ_{DA}, from x^N_{DAN} as φ_{DAN} and x^N_{com} as φ_{com}. Generally φ_{DA} and φ_{DAN} are close to each other, with φ_{DAN} deviating from φ_{DA} towards φ_{obs} for wavelengths 550 and 700 nm. For wavelength 450 nm, φ_{DAN} remains close to $\varphi_o bs$ until approximately 09:20 LT, after which φ_{DAN} follows φ_{DA} with only slight deviations from it. For wavelengths 450 and 550 nm, both φ_{DA} and φ_{DAN} are closer to $\varphi_o bs$ than $\varphi_o bs$. Scattering coefficients calculated from the background state (not shown) differ little from φ_{DAN}. The inclusion

of the nephelometer measurements do, however, have an effect on x^N_{DAN} as a whole over a longer time period. Note that φ_{DAN} is smoother than φ_{DA}, which in turn is smoother than φ_{com}. This indicates that including the nephelometer measurements into the EKF implementation results in a temporally more continuous estimate in the particle size range of 300 - 700 nm.

The state estimate was validated with statistical comparison in **Paper III** and incremental analysis in **Paper IV**. The EKF implementation was also tested with several days from April-May 2007. The independent analysis of each studied day showed that the detailed results presented here to be generally representative of the merits and issues of the use of EKF implementation.

4 Discussion

EKF is presented here as a promising method for estimating particle number size distributions from multiple simultaneous observations. The central merits, challenges and issues concerning EKF implementation in aerosol physics are summarized below.

- The simplified EKF implementation used here was able to estimate a state from simultaneous observations from different detectors. The state estimate fitted all measurements relatively well, including the overlapping measurement ranges. Improvements in the microphysical model, applied parameterizations and error covariance approximations are expected to improve the state estimate.

- Information from prior states contained in the background state affects the state estimate, while the error covariances constrain the state estimate over particle size. The state estimate is thus continuous over both time and particle diameter. However, these reasons also cause the state estimate to react more slowly to sudden changes in the observed state. The impact might be reduced with improved error covariance estimates.

- In addition to the state estimate, EKF also estimates the reliability of the estimate. This feature was not focused on in this work. However, future efforts on the subject should produce better background error covariance approximations, which would in turn allow better approximations on error size-dependencies and to determine the state estimate error covariances.

- The focus here has been on particle number size distribution. The EKF implementation could be extended, though, to also estimate particle composition and properties. This requires additional work and related measurements.

- Finally, it is crucial to remember that ultimately EKF is a statistical tool, and all mathematical methods should be chosen based on the problem at hand. For instance, when the main interest is on the long-term evolution of a particle size distribution, EKF is a potential tool for that purpose. However, if the interest concerns short term changes due to outside influence, then EKF may not be an ideal choice.

5 Review of papers and the author's contribution

Paper I presents the tangent-linear version of UHMA, which is necessary for the EKF implementation, and investigates its limitations. The main limitation for the tangent-linear hypotesis was the dynamical evolution of particles smaller than 20 nm. The tangent-linear hypothesis was established to be valid for measurement cycles of 30 minutes. The author constructed the tangent-linear version of UHMA, performed the simulations and analyzed the results.

Paper II studies the error covariance structures created by UHMA. It shows that inclusion of a propagating background error covariance matrix improves the state estimate opposed to including a static error covariance matrix. The author constructed the EKF implementation, performed the simulations and analyzed the results.

Paper III introduces the EKF implementation as a method to estimate from multiple simultaneous observations. The focus is the general applicability of EKF in aerosol physics, which is tested with observations from a Twin-DMPS instrument. The results were also statistically analyzed. The state estimates were found to generally have less bias than the inversion results and have comparable standard deviation values to the inversion results. Potential improvements to the EKF implementation are discussed. The author compiled the suitable EKF implementation, performed the tests and analyzed the results.

Paper IV expands the EKF implementation to include three different measurement instruments, which all observe different variables. The resulting particle number size distribution estimates appeared to successfully merge the simultaneous observations and are continuous over particle diameter and smooth over time. The author modified the EKF implementation to include the new observations, performed the simulations and analyzed the results.

6 Conclusions

Estimating a particle size distribution from various simultaneous observations remains a challenge in current aerosol physical research. This thesis introduces Extended Kalman Filter (EKF) as a method to produce a statistically optimal estimate of the particle number size distribution from multi-instrument observations. The resulting state estimate is constrained over both time and particle diameter by known aerosol physical processes.

It was established that it is mathematically feasible to apply EKF with the chosen microphysical model and that in a theoretical scenario a properly evolving EKF implementation improves that state estimate. The current EKF implementation was tested by estimating a particle number size distribution from simultaneous measurements from a Differential Mobility Particle Sizer (DMPS), Aerodynamic Particle Sizer (APS) and nephelometer. Both DMPS and APS are size-segregating detectors, which measure size dependent aerosol quantities, and nephelometer is an integrating detector, which measure a single quantity determined by the state. Each instrument provides information of the particle number size distribution in different diameter ranges, with overlapping measurement ranges. Yet each instrument observes variables that cannot be directly compared. A state compared directly from DMPS and APS measurements was used a comparison for the state estimate. The results are here only presented for a single date, 7 May 2007, but these results were established to be well-representative for the period of April-May 2007.

The state estimate was generally continuous over both time and particle diameter. Especially in the overlapping measurement ranges of different instruments, EKF produced a more continues state estimate than the directly combined state. For particle sizes smaller than 4 μm, the state estimates fit the observations from individual size-segregating detectors relatively well. Due to challenges with both the modelling and measurement challenges, the EKF implementation did, however, have difficulties in particle sizes larger than 4 μm. Total number concentration, total volume concentrations and scattering coefficients calculated from state estimate showed less random variation over time than those calculated from the combined state. For scattering coefficients, the measurements show similar continuity than those calculated from the state estimate.

The EKF implementation introduced in this thesis includes several suboptimal as-

sumptions. Still, even this inital version of EKF was able to succesfully incorporate information from very different detectors to succesfully estimate a state fitting all the separate information sources. These results are encouraging towards the application of this method in aerosol physics and support future reserach on the subject.

References

Aalto, P., Hämeri, K., Becker, E., Weber, R., Salm, J., Mäkelä, J.M., Hoell, C., ODowd, C.D., Karlsson, H., Hansson, H.-C., Väkevä, M., Koponen, I.K., Buzorius, G. and Kulmala, M. (2001) Physical characterization of aerosol particles during nucleation events. *Tellus*, 53B:344-358

Ahlquist, N.C. and Charlson, R.J. (1967) A new instrument for evaluating the visual quality of air. *J. Air. Pollut. Control Assoc.* 17:467-469

Anderson, T.L., Covert, D.S., Marshall, S.F., Laucks, M.L, Charlson, R.J., Waggoner, A.P., Ogren, J.A., Caldow, R., Holm, R.L., Quant, F.R., Sem, G.J., Wiedensohler, A., Ahlquist, N.A., and Bates, T.S. (1996) Performance characteristics of a high-sensitivity, three-wavelength total scatter/backscatter nephelometer *J. Atmospheric and Oceanic Technology*, 13:967-986

Anderson, T.L. and Ogren, J.A. (1998) Determining aerosol radiative properties using the TSI 3563 integrating nephelometer. *Aerosol Sci. Tech.*, 29:57-69

Arnott, W.P., Hamasha, K., Moosmüller, H., Sheridan, P.J. and Ogren, J.A. (2005) Towards aerosol light-absorption measurements with a 7-wavelength athalometer: evaluation with a photoacoustic instrument and 3-wavelength nephelometer. *Aerosol Sci. Technol.*, 39:17-29

Barber, P.W. and Hill, S.C. (1990) Light scattering by particles: Computational methos World Scientific Publishing, Singapore

Beuttell, R.G. and Brewer, A.W. (1949) Instruments for the measurement of visual range *J. Sci. Instrum. Phys. Ind.* 26:357-359

Bodhaine, B.A., Ahlquist, N.C. and Schnell, R.C. (1991) Three-wavelength nephelometer suitable for aircraft measurements of background aerosol scattering extinction coefficient. *Atmos. Environ.*, 25A:2267-2276

Buchholz, A. (1995) Rayleigh scattering calculations for the terrestial atmosphere. *Appl. Optics*, 34:2765-2773

Chung, C. E., Ramanthan, V., Carmichael, G., Kulkarn, S., Tang, Y., Adhikary, B., Leung, L. R. and Qian, Y. (2010). Anthropogenic aerosol radiative forcing in Asia

derived from regional models with atmospheric and aerosol data assimilation. *Atmos. Chem. Phys.*, 10:6007-6024

Dubovik, O., Lapyonok, T., Kaufman, Y. J., Chin, M., Ginoux, P., Kahn, R. A., and Sinyuk, A. (2008) Retrieving global aerosol sources from satellites using inverse modelling. *Atmos. Chem. Phys.*, 8:209-250

Elbern, H., Schmidt, H., Talagrand, O., and Ebel, A. (2001) 4D-variational data assimilation with an adjoint air quality model for emission analysis. *Environ. Mod. Software*, 15:539-548

Fiebig, M., Stein, C., Schröder, F., Feldpausch, P. and Petzold, A. (2005). Inversion of data containing information on the aerosol particle size distribution using multiple instruments. *J. Aerosol Sci.*, 36:1353-1372

Fuchs, N. A. (1964) Mechanics of Aerosols. Pergamon, New York

Fuchs, N. A. and Sutugin, A. G. (1971) High-dispersed aerosols, in Topics in Current Aerosol Research. Edited by G. M. Hidy and J. R. Brock, Vol. 2, pp. 1-60, Pergamon, Oxford

Guyon, P., Boucher, O., Graham, B., Beck, J., Mayol-Bracero, O.L., Roberts, G.C., Maenhaut, W., Artaxo, P. and Andreae, M.O. (2003) Refractive index of aerosol particles over the Amazon tropical forest during LBA-EUSTACH. J. Aerosol Sci., 34:883-907

Hand, J.L. and Kreidenweis, S.M. (2002) A new methdod for retrieving particle refractive index and effective density from aerosol size distribution data. *Aerosol Sci. Technol.*, 36:1012-1026

Hand, J. L. and Malm, W. C. (2007). Review of aerosol mass scattering efficiencies from ground-based measurements since 1990. *J. Geophys. Res.*, 112:D16203, doi:10.1029/2007JD008484

Hari, P. and Kulmala, M. (2005) Station for Measuring Ecosystem-Atmosphere Relations (SMEAR II) *Bor. Env. Res.*, 10:315-322

Heintzenberg, J., Wiedensohler, A., Tuch, T. M., Covert, D. S., Sheridan, P., Ogren, J. A., Gras, J., Nessler, R., Kleefeld, C., Kalivitis, N., Aaltonen, V., Wilhelm, R. T., and Havlicek, M. (2006) Intercomparisons and aerosol calibrations of 12 commercial

integrating nephelometers of three manufacturers *J. Atmos. Ocean. Technol.*, 23:902-914

Hinds, W.C. (1999) Aerosol Technology: Properties, behavior and measurements of airborne particles pp. 42-54, New York, Wiley

Hoppel, W. A. (1978) Determination of the aerosol size distribution of the charged fraction of aerosols. *J. Aerosol Sci.*, 9:41-54

Kaipio, J. and Somersalo, E. (2004) Statistical and Computational Inverse Problems Applied Mathematical Sciences, 160, Springer-Verlag. 339 pp. ISBN 0-387-22073-9

Kalman, R. E. (1960) A new approach to linear filtering and prediction problems. *Trans. ASME J. Basic Eng.*, 82D:35-45

Kandlikar, M. and Ramachandran, G. (1999). Inverse methods for analysing aerosol spectrometer measurements: a critical review. *J. Aerosol Sci.*, 30:413-437

Kannosto, J., Virtanen, A., Lemmetty, M., Mäkelä, J. M., Keskinen, J., Junninen, H., Hussein, T., Aalto, P. and Kulmala, M. (2008) Mode resolved density of atmospheric particles. *Atmos. Chem. Phys.*, 8:5327-5337, doi:10.5194/acp-8-5327-2008

Khlystov, A., Stanier, C. and Pandis, S.N. (2010) An Algorithm for Combining Electrical Mobility and Aerodynamic Size Distributions Data when Measuring Ambient Aerosol Special Issue of Aerosol Science and Technology on Findings from the Fine Particulate Matter Supersites Program. *Aerosol Sci. Tech.*, 38:S1:229-238

Korhonen, H., Lehtinen, K. E. J. and Kulmala, M. (2004) Multicomponent aerosol dynamics model UHMA: model development and validation. *Atmos. Chem. Phys.*, 4:471-506

Kulmala, M., Dal Maso, M., Mäkelä, J.M., Pirjola, L., Väkevä, M., Aalto, P.P., Miikkulainen, P., Hämeri, K., and O'Dowd, C.D. (2001) On the formation, growth and composition of nucleation mode particles *Tellus*, 53B:479?490

Kulmala, M., V. Kerminen, T. Anttila, A. Laaksonen, and C. D. O'Dowd (2004) Organic aerosol formation via sulphate cluster activation. *J. Geophys. Res.*, 109:D04205, doi:10.1029/2003JD003961.

Kulmala, M., Lehtinen, K. E. J. and Laaksonen, A.(2006) Cluster activation theory as an explanation of the linear dependence between formation rate of 3 nm particles and sulphuric acid concentration. *Atmos. Chem. Phys.*, 6:787-793

Kulmala, M., Asmi, A., Lappalainen, H. K., Carslaw, K. S., Pöschl,U., Baltensperger, U., Hov, Ø., Brenquier, J.-L., Pandis, S. N., Facchini, M. C., Hansson, H.-C., Wiedensohler, A., and O'Dowd, C. D. (2009) Introduction: European Integrated Project on Aerosol Cloud Climate and Air Quality interactions (EUCAARI) - integrating aerosol research from nano to global scales. *Atmos. Chem. Phys.*, 9:2825-2841, doi:10.5194/acp-9-2825-2009

Lehtinen, K. E. J. and Kulmala, M. (2003) A model for particle formation and growth in the atmosphere with molecular resolution in size. *Atmos. Chem. Phys.*, 2:251-257

Liu, C., Wang, Z. and Zhu, J. (2008) An Ensemble Kalman Filter for severe storm data assimilation over China. *Atmos. Chem. Phys.*, 8:2975-2983

McFiggans, G., Artaxo, P., Baltensperger, U., Coe, H., Facchini, M. C., Feingold, G., Fuzzi, S., Gysel, M., Laaksonen, A., Lohmann, U., Mentel, T. F., Murphy, D. M., O'Dowd, C. D., Snider, J. R. and Weingartner, E. (2006) The effect of physical and chemical aerosol properties on warm cloud activation. *Atmos. Chem. Phys.*, 6:2593-2649

McMurry, P. H. (2000) The History of condensation nucleus counters. Aerosol Sci. Tech., 33:297-322

Moosmüller, H. and Arnott, W.P. (2003) Angular truncation errors in integrating nephelometry. *Rev. Sci. Instrum.*, 74:3492-3501

Myhre, G.(2009) Consistency between satellite derived and modeled estimates of the direct aerosol effect. *Science*, 325:187-190

Paasonen, P., Nieminen, T., Asmi, E., Manninen, H. E., Petäjä, T., Plass-Dülmer, C., Flentje, H., Birmili, W., Wiedensohler, A., Hörrak, U., Metzger, A., Hamed, A., Laaksonen, A., Facchini, M. C., Kerminen, V.-M. and Kulmala, M. (2010) On the roles of sulphuric acid and low-volatility organic vapours in the initial stages of atmospheric new particle formation. *Atmos. Chem. Phys.*, 10:11223-11242

Peters, T.M. and Leith, D. (2003) Concentration measurement and counting efficiency of the aerodynamic article sizer 3321. *J. Aerosol Sci.*, 34(5):627-634

Petzold, A., Rasp, K., Weinzierl, B., Esselborn, M., Hamburger, T., Dörnbrack, Kandler, K., Schütz, L., Knippertz, P., Fiebig, M., and Virkkula, A. (2009) Saharan dust absorption and refractive index from aircraft-based observations during SAMUM 2006. *Tellus B*, 61(1):118-130

Petäjä, T., Mauldin, III, R. L., Kosciuch, E., McGrath, J., Nieminen, T., Paasonen, P., Boy, M., Adamov, A., Kotiaho, T. and Kulmala, M. (2009) Sulfuric acid and OH concentrations in boreal forest site. *Atmos. Chem. Phys.*, 9:7435-7448

Pitz, M., Birmili, W., Schmid, O., Peters, A., Wichmann, H.E. and Cyrys, J. (2008) Quality control and quality assurance for particle size distribution measurements at an urban monitoring station in Augsburg, Germany. *J. Environ. Monit.*, 10:1017-1024

Pope, C. A. and Dockery D. W. (2006). Health effects of fine particulate air pollution: lines that connect. *J. Air & Waste Manage. Assoc.*, 56:709-742

Quant, F.R., Caldow, R., Sem, G.J. and Addison, T.J. (1992) Performance of condensation particle counters with three continuous-flow designs. *J. Aerosol Sci.*, 23:405-408

Rannik, U., Aalto, P., Keronen, P., Vesala, T. and Kulmala, M. (2003) Interpretation of aerosol particle fluxes over a pine forest: Dry deposition and random errors. *J. Geophys. Res.*, 108(D17):4544, doi:10.1029/2003JD003542

Saarikoski, S., Mäkelä, T., Hillamo, R., Aalto, P., Kerminen, V.-M., and Kulmala, M. (2005) Physico-chemical characterization and mass closure of size-segregated atmospheric aerosols in Hyytiälä, Finland. *Boreal Environ. Res.*, 10:385-400

Schutgens, N.A.J., Miyoshi, T., Takemura, T., and Nakajima, T. (2010) Sensitivity tests for an ensemble Kalman Filter for aerosol assimilation. *Atmos. Chem. Phys.*, 10:6583-6600

Sekiyama, T.T., Tanaka, T.Y., Shimizu, A. and Miyoshi, T. (2010) Data assimilation of CALIPSO aerosol observations. Atmos. Chem. Phys., 10:39-49

Sihto, S.-L., Kulmala, M., Kerminen, V.-M., Dal Maso, M., Petäjä, T., Riipinen, I., Korhonen, H., Arnold, F., Janson, R., Boy, M., Laaksonen, A. and Lehtinen, K. E. J. (2006) Atmospheric sulphuric acid and aerosol formation: implications from atmospheric measurements for nucleation and early growth mechanisms. *Atmos. Chem. Phys.*, 6:4079-4091

Shen, S., Jaques, P.A., Zhu, Y., Gellar, M.D. and Sioutas, C. (2002) Evaluation of the SMPS-APS system as a continuous monitor for measuring PM2.5, PM10 and coarse (PM2.5-10) concentrations. *Atmos. Environ.*, 36(24):3939-3950

Stolzenburg, M. (1988) An ultrafine aerosol size distribution system. PhD thesis, University of Minnesota, Minneapolis, MN

Stolzenburg, M., and McMurry, P. (1991) An ultrafine aerosol condensation nucleus counter. *Aerosol Sci. Technol.*, 14:48-65

Stolzenburg, M. and McMurry, P. (2008) Equations Governing Single and Tandem DMA Configurations and a New Lognormal Approximation to the Transfer Function. *Aerosol Sci. Technol.*, 42:6:421-432

Tombette, M., Mallet, V. and Sportisse, B. (2009) PM10 data assimilation over Europe with the optimal interpolation method. *Atmos. Chem. Phys.*, 9:57-70

Virkkula, A., Koponen, I. K., Teinilä, K., Hillamo, R., Kerminen, V.-M., and Kulmala, M. (2006) Effective real refractive index of dry aerosols in the Antarctic boundary layer. *Geophys. Res. Lett.*, 33(6):L06805, 10.1029/2005GL024602

Virkkula, A., Backman, J., Aalto, P.P., Hulkkonen, M., Riuttanen, L., Nieminen, T., Dal Maso, M., Sogacheva, L., De Leeuw, G. and Kulmala, M. (2011) Seasonal cycle, size dependencies and source analyses of aerosol optical properties at the SMEAR II measurement station in Hyytiälä, Finland. *Atmos. Chem. Phys.*, 11:4445-4468, doi:10.5194/acp-11-4445-2011

Volckens, J.A.E. and Peters, T.M. (2005) Counting and particle transmission efficiency of the aerodynamic particle sizer. *J. Aerosol Sci.*, 36:1400-1408

Voutilainen, A. (2001) Statistical inversion methods for the reconstruction of aerosol size distributions PhD thesis, University of Kuopio, Finland

Vuollekoski, H., Nieminen, T., Paasonen, P., Sihto, S.-L., Boy, M., Manninen, H., Lehtinen, K. E. J., Kerminen, V.-M. and Kulmala, M. (2010) Atmospheric nucleation and initial steps of particle growth: numerical comparison of different theories and hypotheses. *Atmos. Res.*, 90:229-236

Wiedensohler, A. (1988) Die bipolare Diffusionsaufladung von Partikeln in chemisch trägen Reinstgasen. PhD thesis, University of Duisburg, Germany.

Wiedensohler, A., Birmili, W., Nowak., A., Sonntag, A., Weinhold, K., Merkel, M., Wehner, B., Tuch, T., Pfeifer, S., Fiebig, M., Fjäraa, A. M., Asmi, E., Sellegri, K., Venzac, H., Villani, P., Laj, P., Aalto, P., Ogren, J. A., Swietlicki, E., Roldin, P., Williams, P., Quincey, P., Hüglin, C., Schmidhauser, R., Gysel, M., Weingartner, E., Riccobono, F., Santos, S., Grüning, S., Fallon, K., Beddows, D., Monaha, C., Marioni, A., Horn, H.-R., Keck, L., Jiang, J., Scheckman, J., McMurry, P. H., Deng, Z. and Zhao, C. S. (2010) Particle mobility size spectrometers: harmonization of technical standards and data structure to facilitate high quality long-term observations of atmospheric particle size distributions. *Atmos. Meas. Tech. Discuss.*, 3:5521-5587

Winklmayr, W., Reischl, G., Lindner, A., and Berner, A. (1991) A new electromobility spectrometer for the measurement of aerosol size distributions in the size range from 1 to 1000 nm. *J. Aerosol Sci.*, 22:289-296